Received April 13, 2022, accepted April 27, 2022, date of publication May 9, 2022, date of current version May 12, 2022.

Digital Object Identifier 10.1109/ACCESS.2022.3173309

Numerical Analysis and Experimental Study of the Laser Cleaning of Ceramic Insulator Contamination

XIANQIANG LI[1], (Member, IEEE), JI TIAN[1], ZHIYUAN MA[2], WENCHUANG ZHOU[1], AND YUANCHENG QIN[1]

[1]School of Automation, Wuhan University of Technology, Wuhan 430070, China
[2]State Grid Suzhou Power Supply Company, Suzhou 234000, China

Corresponding author: Xianqiang Li (lxq@whut.edu.cn)

This work was supported by the Guangdong Power Grid Co., Ltd. under Grant 030700KK52180143.

ABSTRACT Contamination flashover of insulators is one of the main threats to the safety of power systems, and regular cleaning of insulator surface pollution is an effective solution to this problem. In this paper, the laser cleaning of ceramic insulators is studied via simulations and experiments. The adhesion between a contamination layer and an insulator surface is estimated. A laser cleaning model for contaminated insulators is established, and a numerical analysis of the thermal stress field distribution characteristics of laser cleaning is carried out. Various factors that affect the thermal stress field distribution, including the laser power, laser scanning speed and thickness of the contamination layer, are also analysed. The optimal cleaning parameters for the best performance of laser cleaning are obtained through simulation and experiments. The result shows if the equivalent salt deposit density (ESDD) is 0.05 mg/cm^2, and the nonsoluble deposit density (NSDD) is 0.25 mg/cm^2, the best cleaning effect could be achieved when the laser power is 100 W and the scanning speed reached 6000 mm/s.

INDEX TERMS Ceramic insulator, contamination, laser cleaning, thermal stress.

I. INTRODUCTION

Outdoor insulators are always exposed to air, and contamination particles can accumulate on insulator surfaces. A contamination layer can gradually formulate, leading to a potential flashover hazard and even a large-scale power outage, especially in humid conditions, such as fog, haze, dew and light rain [1], [2]. Insulator contamination flashover is a severe threat to the reliability and safety of power systems. According to historical statistics, in addition to lightning hazards, insulator contamination flashover is the second top hazard for a power grid, but the damage is approximately 10 times more than that of a lightning hazard [3]. Therefore, effective measures must be implemented to remove contamination from insulator surfaces in a timely manner to ensure the safety and reliability of power systems.

Many methods have been used to remove contamination, such as live water washing [4]–[7], dry ice cleaning [8]–[10], and detergent cleaning [11]. These methods have achieved a certain cleaning effect, but there are also some deficiencies. Water washing requires a large amount of deionized water and has a risk of adjacent flashover in substations. Dry ice washing wastes a large amount of carbon dioxide, which is harmful to the environment. Detergent cleaning uses organic solvents, which may cause environmental pollution and corrosion of metal fittings.

Compared to traditional cleaning methods, laser cleaning technology has the merits of safety, high efficiency, noncontact, environmentally friendly and noncorrosive and has been widely applied in many fields [12]. In [13], a theoretical model for laser cleaning of microparticles was established and took the factors of adhesion and thermal expansion into account. N. Arnold [14] found that particles can be eliminated from a solid surface when either the elastic energy, inertial force or kinetic energy exceeds the adhesion potential energy. Different laser pulse widths may affect the energy delivered to the insulator surface and may eventually affect the performance of dry laser cleaning. Liu *et al.* [15] studied the distribution characteristics of the temperature field during laser cleaning of paint and the influence of laser

The associate editor coordinating the review of this manuscript and approving it for publication was Guijun Li.

parameters on the temperature field. It was found that the surface temperature of a paint film increased linearly with increasing laser energy density and laser repetition frequency. Gao *et al.* [16] studied the laser cleaning effects on an aluminium alloy surface paint layer through experiments. The results showed that the cleaning effect was optimal under the experimental conditions with a laser energy density of 25 J/cm^2 and an overlap rate of 50%. In [17], [18], the laser cleaning of aluminium alloy surface oxide and aluminium surface paint layers was studied. It was found that thermal stress and laser-induced plasma contribute to the cleaning of the paint and oxide layers. In [19], [20], the effects of laser attributions, such as the power density, pulse frequency and overlapping rate of adjacent scans, on the cleaning effect were studied with experiments. From the point of view of laser ablation and vibration effects, Xue *et al.* [21] studied the influence of power density on the cleaning effect. Ye and Qi of the China University of Geosciences focused on the application of laser cleaning technology to the cleaning of pollutants on the surface of stone cultural relics. Simulation and experimental methods have been used to verify that the laser cleaning method is effective and that there are no adverse impacts on stone cultural relics [22], [23]. In [24]–[26], laser cleaning was applied to various fields, such as mould cleaning, rust removal and insulator room temperature vulcanized (RTV) coating cleaning. However, there are few reports on the application of laser cleaning of insulator contamination in power systems.

In this paper, laser cleaning of ceramic insulators is studied via simulations and experiments. The stress field distribution characteristics and relevant factors during laser cleaning are analysed. This paper is organized as follows. Theoretical analyses, including the interactions between a laser and ceramic materials and a laser cleaning mechanism and an adhesion force, are elaborated in Section II. Section III develops the laser cleaning numerical model for the simulation and includes a mathematical model for the laser heat source and an insulator adhesion contamination model. Section IV describes the distribution characteristics of the thermal stress field during laser cleaning. Section V discusses the influencing factors of the stress distribution, including the laser power, scanning speed and thickness of the contamination layer. The theoretical parameter range for effective cleaning was obtained. Section VI explores the cleaning effect experimentally. Finally, the conclusions are summarized in Section VII.

II. THEORETICAL ANALYSIS

A. INTERACTION BETWEEN A LASER AND MATERIALS

A schematic of the laser cleaning ceramic insulator is shown in Fig. 1. As a certain kind of electromagnetic wave, a laser satisfies the Maxwell equation in the process of propagation. The wave equation of the laser electric vector is given by [27]:

$$\nabla^2\vec{E} - \mu_r\mu_0\sigma\frac{\partial\vec{E}}{\partial t} - \mu_r\mu_0\varepsilon_r\varepsilon_0\frac{\partial^2\vec{E}}{\partial^2 t} = 0 \tag{1}$$

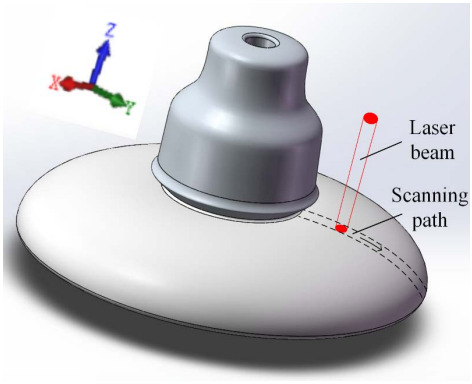

FIGURE 1. Schematic diagram of laser cleaning of a ceramic insulator.

where μ_r, μ_0 and σ are the relative permeability of the material, the vacuum permeability of the material and the conductivity of the material, respectively. ε_r is the relative dielectric constant of the material, and ε_0 is the vacuum dielectric constant.

When a laser beam propagates along the z-axis in isotropic materials, the change rate of the laser beam in the z direction is larger than that in the x and y directions. Then, equation (2) can be simplified as follows:

$$\frac{\partial^2\vec{E}}{\partial^2 z} - \mu_r\mu_0\sigma\frac{\partial\vec{E}}{\partial t} - \mu_r\mu_0\varepsilon_r\varepsilon_0\frac{\partial^2\vec{E}}{\partial^2 t} = 0 \tag{2}$$

The solution of the equation is given by

$$\vec{E} = \vec{E}_0\exp\left[i\omega\left(\frac{z}{v} - t\right)\right] \tag{3}$$

where ω is the frequency of the electric field in the medium and v is the wave velocity.

In the process of laser propagation in the material, the laser intensity $I(z)$ at a distance z from the surface is given by

$$I(z) = \vec{E}\vec{E}^* = E_o^2\exp(-2\omega\kappa z/c) = I_0\exp(-\alpha_0 z) \tag{4}$$

where I_0 is the initial light intensity and α_0 is the absorption coefficient of the material.

Considering the reflection from the material surface to the laser [27], equation (4) can be expressed as follows:

$$I(z) = (1-R)I_0\exp(-\alpha_0 z) \tag{5}$$

where R is the reflectivity. According to the Lorentz damping oscillator model, the internal energy of the ceramic material increases after the internal oscillator absorbs the laser material.

Under the action of heat conduction, the temperature will rise in a certain area of laser irradiation. The temperature distribution $T(x, y, z; t)$ in this area is expressed by the Fourier heat conduction equation [23]

$$\rho c\frac{\partial T(x,y,z;t)}{\partial t} = k\left(\frac{\partial^2 T}{\partial x^2} + \frac{\partial^2 T}{\partial y^2} + \frac{\partial^2 T}{\partial z^2}\right) + F(x,y,z;t) \tag{6}$$

where ρ, c and k are the density, specific heat capacity and heat conductivity of the material, respectively, and $F(x, y, z; t)$ is the internal heat source.

The nonuniform temperature field and deformation of materials are formed under laser irradiation. Due to the constraints around the material, deformation cannot occur freely, resulting in a large thermal stress. Assuming that the material is isotropic and there is no phase transformation, the calculation of thermal stress conforms to the generalized Hooke's law, as shown by the following equations [27]:

$$\begin{cases} \sigma_x = \dfrac{E[(1-\mu)\varepsilon_x + \mu(\varepsilon_y + \varepsilon_z)]}{(1-2\mu)(1+\mu)} - \dfrac{E\alpha\Delta T}{1-2\mu} \\ \sigma_y = \dfrac{E[(1-\mu)\varepsilon_y + \mu(\varepsilon_x + \varepsilon_z)]}{(1-2\mu)(1+\mu)} - \dfrac{E\alpha\Delta T}{1-2\mu} \\ \sigma_z = \dfrac{E[(1-\mu)\varepsilon_z + \mu(\varepsilon_x + \varepsilon_y)]}{(1-2\mu)(1+\mu)} - \dfrac{E\alpha\Delta T}{1-2\mu} \\ \tau_{xy} = \dfrac{E}{2(1+\mu)}\gamma_{xy},\ \tau_{yz} = \dfrac{E}{2(1+\mu)}\gamma_{yz} \\ \tau_{zx} = \dfrac{E}{2(1+\mu)}\gamma_{zx} \end{cases} \tag{7}$$

where E is the elastic modulus; μ is Poisson's ratio; ε_x, ε_y, ε_z are three-dimensional positive strains; γ_{xy}, γ_{yz}, γ_{zx} are three-dimensional shear strains; α is the linear expansion coefficient of the material; and ΔT is the temperature variation, and $\Delta T = T(x, y, z; t) - T(x, y, z; 0)$.

B. CLEANING MECHANISM

In the process of cleaning insulator contamination by a laser, the temperature of the irradiated surface rises rapidly due to the high power of the short pulse laser, resulting in large thermal stress. It has been shown that when the thermal stress is enough to overcome the adhesion force, the pollutants can be separated from the surface of the substrate [13], [28], [29].

A process diagram of the laser cleaning of contamination is shown in Fig. 2. With laser irradiation, the surface temperature of the material rises rapidly, and then a large thermal stress appears, which is the source of the cleaning force. Moreover, the instantaneous thermal stress forms a stress wave that propagates internally and creates a strong vibration effect on the substrate surface. Under the effect of thermal stress and vibration, the contamination layer is crushed and further separated from the substrate surface. If the cleaning force is enough to overcome the adhesion force, the contamination layer can be exfoliated from the substrate surface.

C. ADHESION FORCE CALCULATION

A tight crystalline substance on an insulator surface was formulated by a large amount of contamination particle accumulation, as shown in Fig. 3. The adhesion force represents the tightness between the contamination and the insulator surface. The adhesion force includes many forces, such as Van der Waals forces, electrostatic forces, and gravity [30]. Previous studies have shown that Van der Waals

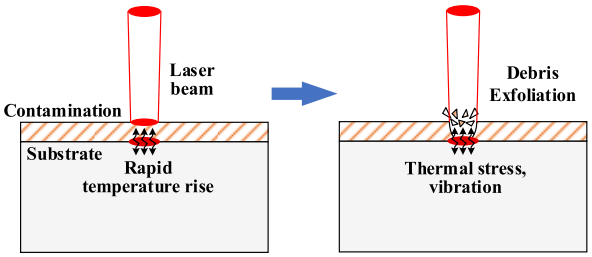

FIGURE 2. Schematic diagram of the laser cleaning principle.

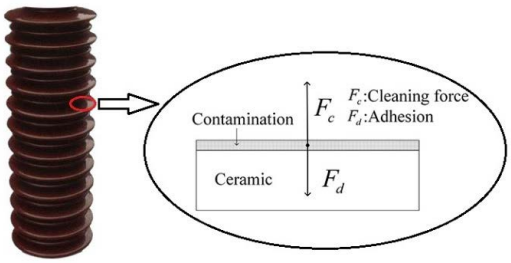

FIGURE 3. Schematic of a contaminated insulator.

forces are dominant and are several orders of magnitude higher than other forces [3], [31]. The attractive Van der Waals force between an ideal spherical particle and a flat solid surface is given by [32].

$$F_{v1} = \frac{h_{12}R}{8\pi z^2} \tag{8}$$

where R, h_{12} and z are the radius of the contamination particles, the material-dependent Van der Waals constant and the distance between the contamination particles and insulator surface, respectively.

In fact, the contact area will increase due to the deformation of the contamination particles, and the Van der Waals force will be increased, as shown by the following equation [32]:

$$F_{v1} = \frac{h_{12}R}{8\pi z^2} \tag{9}$$

where δ is the radius of the adherent surface. Therefore, the total Van der Waals force is given by

$$F_v = \frac{h_{12}R}{8\pi z^2} + \frac{h_{12}\delta^2}{8\pi z^3} \tag{10}$$

Then, the force on the contact surface per unit area can be expressed as follows [32]:

$$f_v = \frac{h_{12}R}{8\pi^2 z^2\delta^2} + \frac{h_{12}}{8\pi^2 z^3} \tag{11}$$

For large deformations, such as $\delta/R \geq 10\%$, the approximate Van der Waals force per unit area is given by

$$f_v \approx \frac{h_{12}}{8\pi^2 z^3} \tag{12}$$

The Van der Waals constant h_{12} is related to the Hamaker constants of the materials, as shown in the following

TABLE 1. Hamaker constants of materials.

Material	Ceramic insulator (A_{22})	Contamination (A_{11})	Air (A_{33})
Hamaker constant	8.75×10^{-20} J	6.60×10^{-20} J	1.94×10^{-20} J

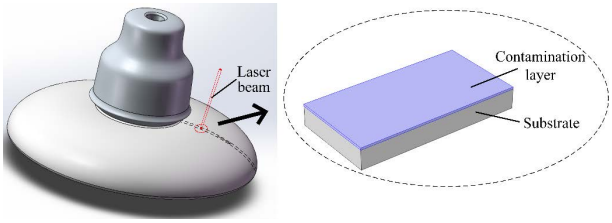

FIGURE 4. Schematic diagram of insulator cleaning by a laser.

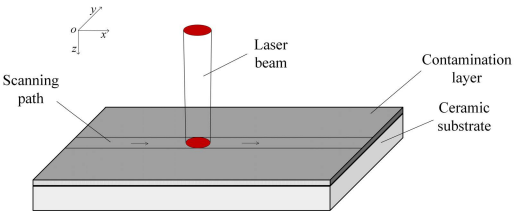

FIGURE 5. Model of a laser cleaning an insulator.

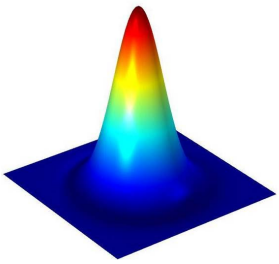

FIGURE 6. Model of the laser heat source.

equation [33]:

$$h_{12} = \frac{4}{3}\pi A_{12} \tag{13}$$

where A_{12} is the Hamaker coefficient, which refers to the constant of two materials in contact with each other and is given as follows [33]:

$$A_{12} = \left(\sqrt{A_{11}} - \sqrt{A_{33}}\right) \times \left(\sqrt{A_{22}} - \sqrt{A_{33}}\right) \tag{14}$$

where A_{11} is the Hamaker constant of contamination, A_{22} is the Hamaker constant of the ceramic insulator material, and A_{33} is the Hamaker constant of air. The Hamaker constants of the materials are shown in Table 1.

Referring to the constants in Table 1, A_{12} could be calculated to be 1.8×10^{-20} J by (14). Furthermore, h_{12} is 7.7×10^{-20} J. Therefore, according to (12), assuming that the distance z is 4×10^{-10} m [13], the adhesion force per unit area is obtained as 15.2 MPa. According to the analysis of the mechanism for the laser cleaning of contamination, if the thermal stress f_c caused by laser irradiation is greater than the adhesion force f_v, the contamination layer can be separated. Therefore, the effective cleaning criterion is $f_c > f_v = 15.2$ MPa.

III. NUMERICAL MODELS OF LASER CLEANING

In the laser cleaning process, the laser beam is focused on the field mirror, and the radius of the spot is small, as shown in Fig. 4. In practice, the laser beam is a focused spot with a radius ranging from 1 mm to several micrometers to achieve a high energy concentration. The thermal impact area of the laser during cleaning is focused around the spot area. The laser has negligible impacts on temperature and thermal stress of the adjacent areas. Therefore, a parallel hexahedral domain on the scan path is captured as the object of study, as shown in Fig. 4. The surface of the model is the contamination layer, and the interior is the ceramic insulator layer.

A schematic diagram of laser cleaning is shown in Fig. 5. The laser beam moves along a certain track at a constant speed during the cleaning process. The following assumptions are made in the model: it is assumed that (1) the contamination layer is uniformly distributed, (2) the materials of both the contamination layer and the ceramic layer are isotropic, and (3) the upper surface of the model is the heat exchange surface. The other surfaces are adiabatic since there is no exchange of heat.

In the process of using a 1064 nm laser to clean ceramic insulators, the penetration depth of infrared light into the contamination layer is very small. The absorption and heat conversion of the laser photons by the contamination layer is very fast and is only approximately $10^{-11} - 10^{-10}$ s, which is far less than the pulse width of the laser. Therefore, in the model, when the contamination layer absorbs the laser, the laser can be considered as a surface heat source. For a better cleaning effect, the laser beam is usually the fundamental mode output, and the intensity distribution obeys a Gaussian distribution, as shown in Fig. 6.

Considering the movement of the laser beam during the cleaning process, the laser dynamic mathematical model is shown in equation (15) [23]:

$$I(x, y, t) = \frac{AP}{\pi R^2} e^{\frac{-[(x-vt)^2+y^2]}{R^2}} \tag{15}$$

where I is the laser power density; A is the absorption coefficient of the material impacted by the laser and is set as 0.8; P is the laser power; R is the radius of the laser spot; and v is the laser moving speed.

The temperature field $T(x, y, z, t)$ under laser irradiation is calculated by equation (6). The initial temperature is set as $T_0 = 293$ K. The air exchange and heat radiation on the upper surface of the model are considered, and other surfaces are

TABLE 2. Physical parameters of material.

Parameters	Contamination layer	Substrate layer
Density (kg*m^{-3})	1660	2400
Specific heat capacity (J*(kg·°C)$^{-1}$)	900	816
Thermal conductivity (W*m^{-1}*K^{-1})	2.1	1.86
Linear expansion coefficient (K^{-1})	3.91×10^{-6}	5.66×10^{-6}
Poisson ratio	0.17	0.2
Elastic modulus (GPa)	55	76.5

insulated. The boundary condition of the model is set as [16]

$$\begin{cases} k\dfrac{\partial T}{\partial n}\Big|_{\Gamma_1} = 0 \\ -k\dfrac{\partial T}{\partial n}\Big|_{\Gamma_2} = h(T_f - T) + \sigma\varepsilon(T_f^4 - T^4) \end{cases} \tag{16}$$

where Γ_1 is the boundary of $x = \pm W/2$, $y = \pm L/2$ and $z = 0$; n is the external normal of the boundary of the model; Γ_2 is the boundary of $Z = H$ (W, L and H are the length, width and height of the model, respectively); h is the convective heat transfer coefficient between the model and the air. $h = 12.5$ W/(m$^2\cdot$K); T_f is the reference temperature and is 293 K; σ is the Stefan Boltzmann coefficient; and ε is the specific emissivity of the material.

The calculation of spatio thermal stress is based on the generalized Hooke's law shown in equation (7). Taking insulators in the inland areas of China as an example, the main component of natural contamination is SiO_2, which accounts for more than 50% [34] of the contamination layer. Therefore, the physical properties of the contamination layer are those of SiO_2. The thermal physical parameters of the models are shown in Table 2.

IV. CHARACTERISTICS OF THE THERMAL STRESS DISTRIBUTION

Based on the finite element calculation software (COMSOL, version number 5.4), the structural mechanics module and solid heat transfer module are taken into account. The simulation parametric values are set as follows: the laser power is 100 W, the scanning speed is 8000 mm/s, and the thickness of the contamination layer is 50 μm.

In the process of laser scanning, the thermal stress distribution on the interface (the contact surface of the contamination layer and the substrate layer) is shown in Fig. 7. The high thermal stress area is concentrated in the centre, and the surrounding thermal stress decreases gradually. The peak value is 10.2 MPa at t = 0.5 ms. At t = 1 ms, the peak thermal stress reaches 16.8 MPa, and the high stress area increases significantly during laser scanning. At this time, the thermal stress is sufficient to overcome the adhesion, and thus, the contamination layer will be removed.

The variation in thermal stress with time in the laser cleaning process is shown in Fig. 8. The point at x = 2.4 mm

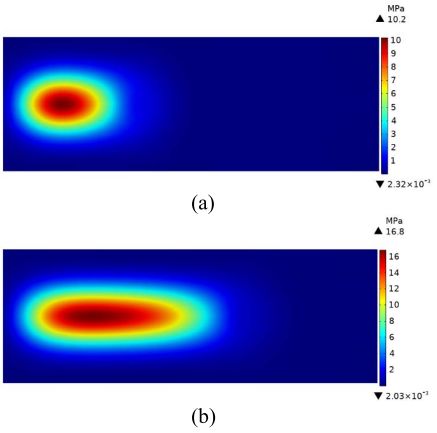

FIGURE 7. Thermal stress distribution on the interface. (a) t = 0.5 ms; (b) t = 1 ms.

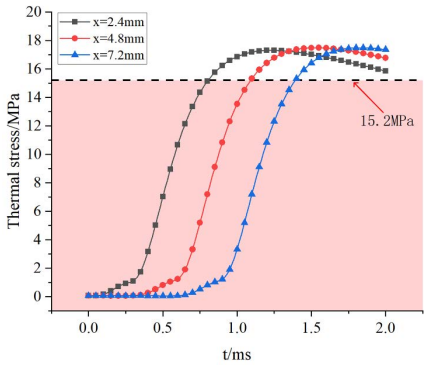

FIGURE 8. Thermal stress at points on the scanning path.

(i.e., when t = 0.3 ms, the spot centre arrives at the point) shows that the change in thermal stress is divided into four stages. The thermal stress rises slowly from 0 ~ 0.3 ms. Then, the thermal stress rises rapidly when the spot centre reaches this point, i.e., from 0.3 ~ 0.8 ms, and the thermal stress value reaches the cleaning threshold of 15.2 MPa at approximately 0.75 ms. After 0.8 ms, the stress value starts to rise slowly until it reaches a peak value of 17.29 MPa. The thermal stress decreases slowly after reaching the peak. The two points at x = 4.8 mm and 7.2 mm have similar thermal stress trends as the point at x = 2.4 mm, indicating that the stress trends at individual points on the scan path are consistent at different times.

The distribution of thermal stresses along the y-axis direction at the interface is shown in Fig. 9. The stress distribution obeys a Gaussian distribution. The thermal stress is symmetrical along the centre, and the maximum stress value is at the centre. The stresses on both sides gradually decrease. In the centre and nearby areas, the thermal stress value is greater than the cleaning threshold, indicating that the contaminated layer can be effectively cleaned. However, the thermal stress at a location slightly away from the centre is less than the cleaning threshold, and the contaminated layer cannot be effectively cleaned.

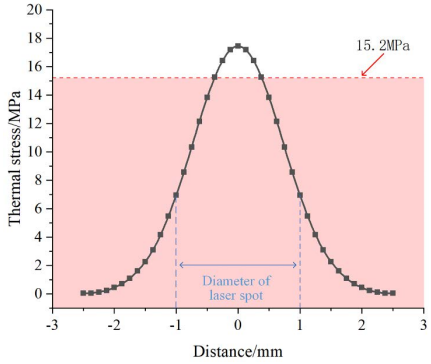

FIGURE 9. Thermal stress distribution along the y-axis direction.

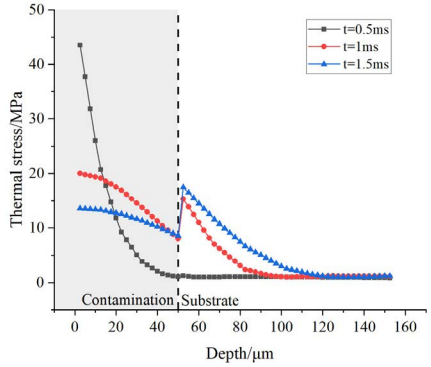

FIGURE 10. Thermal stress distribution along the depth direction.

The thermal stress distribution along the depth direction (at x = 4 cm) is shown in Fig. 10. At 0.5 ms, the stress on the contamination surface increases rapidly as the laser scans this point but decreases rapidly in the depth direction. Thermal stress on the substrate surface hardly increases at this time. At t = 1 ms, with the inward conduction of temperature, the internal thermal stress increases significantly, while the thermal stress of the contamination surface decreases considerably compared to the stress at 0.5 ms. The thermal stress increases from 8 MPa to approximately 15 MPa at a depth of 50 μm at 1 ms. There is a sudden increase in the thermal stress on the interface. The reason is that the thermal expansion coefficient and the elastic modulus of the substrate material are larger than those of the contamination layer, resulting in a sudden increase in the thermal stress, which also contributes to the removal of the contamination layer from the substrate layer.

V. INFLUENCING FACTORS OF THE STRESS DISTRIBUTION

A. LASER POWER

The power of the laser is one of the main factors affecting the distribution of the stress field. To analyse the influence of laser power, the simulation conditions are set as follows. The laser scanning speed is 8000 mm/s, the thickness of the contamination layer is 50 μm, and the laser power values are set to 80 W, 90 W, 100 W, 110 W, and 120 W.

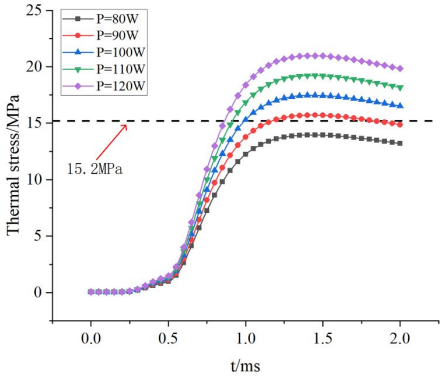

FIGURE 11. Thermal stress on the interface with different laser power values.

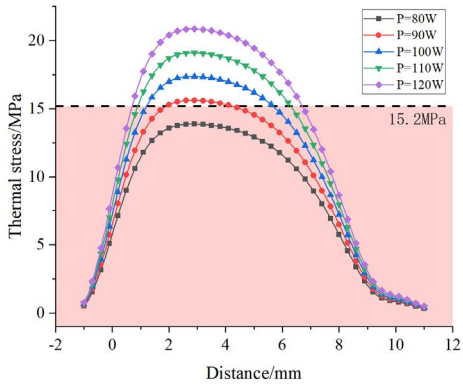

FIGURE 12. Stress distribution along the x-axis with different laser power values.

The thermal stress on the interface with different laser power values is shown in Fig. 11. It is apparent that the rising speed and peak value of thermal stress increase with increasing laser power. With a laser power of 80 W, the thermal stress value is always below the cleaning threshold, and contamination cannot be removed. When the power increases to 90 W, the thermal stress increases further, and the cleaning threshold is exceeded for a period of time near the peak of the thermal stress, indicating that the contamination layer will be effectively cleaned at this power value. The simulation results show that the higher the laser power is, the better the cleaning effect. It should also be considered that the laser power should not be too high; otherwise, it will cause damage to the substrate material.

The thermal stress distribution along the x-axis at t = 1.3 ms with different laser powers is shown in Fig. 12. The position at x = 0 is where the laser starts scanning, and the thermal stress value is small at this location. The thermal stress value rises rapidly in the range of 0 ∼ 2 mm and peaks near x = 2.5 mm. The peak thermal stress exceeds the cleaning threshold when the laser power reaches 90 W and above, which is consistent with the above analysis. The thermal stress decreases gradually in the range of 6 mm to 10 mm and decreases to zero at the end of the axis.

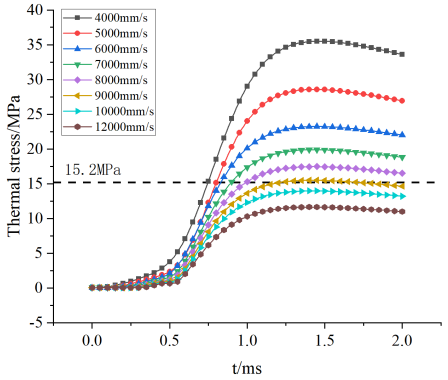

FIGURE 13. Thermal stress on the interface at different scanning speeds.

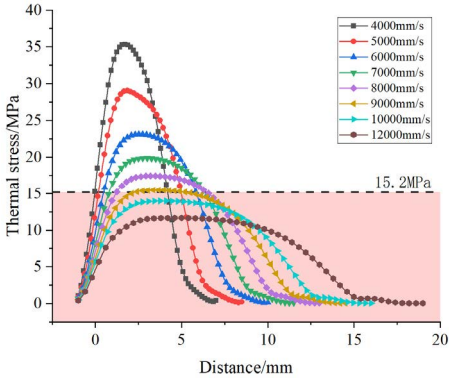

FIGURE 14. Thermal stress distribution along the x-axis at different scanning speeds.

B. SCANNING SPEED

The scanning speed of the laser affects the duration of radiation at each point and directly affects thermal stress in the cleaning process. The effect of the laser scanning speed on the thermal stress is studied in this section. The simulation parameters are set as follows: the laser power is 100 W, the thickness of the contamination layer is 20 μm, and the scanning speed increases in the range of 4000 mm/s to 12000 mm/s.

The point x = 4 mm on the scanning axis of the interface is selected for the study (i.e., the laser spot centre point at 0.5 ms), and the change in thermal stress at this point during the laser scanning process is shown in Fig. 13. The thermal stress rises rapidly when the laser scans this point. When the scanning speed is slow, the temperature rises faster, and the maximum thermal stress is larger. By comparing the thermal stress with the cleaning threshold, it can be found that the thermal stress curve is always less than the cleaning threshold at 10000 mm/s and 12000 mm/s. When the rate is reduced to 9000 mm/s, the peak thermal stress is 15.5 MPa, which is just above the cleaning threshold. When the rate is further reduced, the thermal stress increases further. The peak of the thermal stress reaches 35.5 MPa when the scanning speed is 4000 mm/s.

The distribution of the thermal stress along the x-axis at 1.3 ms with different scanning speeds is shown in Fig. 14. It can be seen that there are significant variations in the distribution of the thermal stress at different speeds. The slower the scanning speed is, the faster the rise rate of the thermal stress value and the larger the peak thermal stress value. When the scanning speed is increased gradually, the peak thermal stress decreases gradually, but the scanning length per unit time is longer, which is helpful to improve the cleaning efficiency. When the scanning speed is too high, the peak thermal stress is always below the cleaning threshold, which results in the contamination layer not being removed effectively.

C. THICKNESS OF THE CONTAMINATION LAYER

In the process of laser cleaning, the high temperature on the contamination layer surface is gradually transmitted

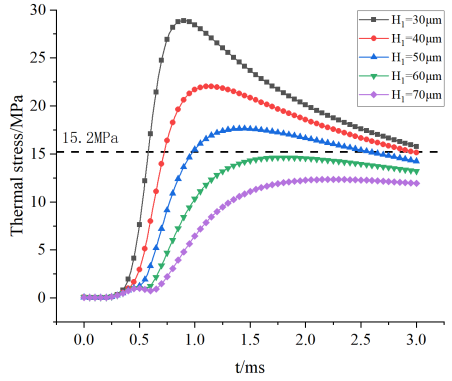

FIGURE 15. Thermal stress on the insulator surface with different contamination layer thicknesses.

to the interior. The thickness of the contamination layer has a significant influence on the temperature rise and the thermal stress of the interface. To study the influence of the thickness of the contamination layer on the thermal stress, the simulation parameters are set as follows: the laser power is 100 W, the scanning speed is 8000 mm/s, and the thicknesses of the contamination are set to 30 μm, 40 μm, 50 μm, 60 μm, and 70 μm.

The thermal stress at the point (x = 4 cm) on the laser scanning path is shown in Fig. 15. When the contamination layer is thin, the thermal stress rises rapidly after the laser scanning reaches this point. With a thickness of 30 μm, the thermal stress rises rapidly to 28.7 MPa in the range of 0.3 ms to 0.95 ms and then begins to decrease. However, when the thickness of the contamination layer is 70 μm, the thermal stress increases slowly. Thermal stress decreases at a slower rate when the contamination layer is thicker.

The stress distribution along the x-axis (at 2.5 ms) is shown in Fig. 16. If the contamination layer is thin, the thermal stress at the point scanned by the laser rises rapidly, falls rapidly after scanning, and then falls slowly. When the contamination layer is thick, the thermal stress rise is very slow, and the decrease is also relatively slow. When the thickness of the contamination layer is too thick, the thermal

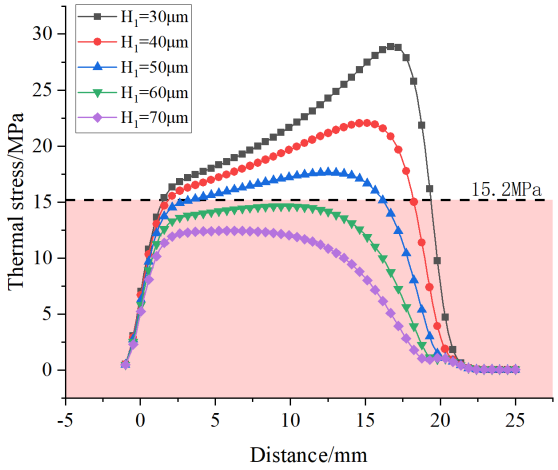

FIGURE 16. Stress distribution along the x-axis with different contamination layer thicknesses.

stress value is always smaller than the cleaning threshold, and the contamination layer cannot be cleaned effectively. When the contamination layer is thinner, the thermal stress value is higher and the cleaning force is greater, which makes it easier to remove the contamination layer.

VI. OPTIMAL PARAMETERS RANGE SELECTION FOR EFFECTIVE CLEANING

From the above analysis, it is clear that the laser cleaning effect is affected by the laser power, scanning speed and the thickness of contamination. Considering these factors together, the parameter interval for effective cleaning with different thicknesses of contamination is obtained. Fig. 17 shows the thermal stress values with 60 μm contamination during laser cleaning. From the figure, it can be seen that the area where the cleaning threshold of 15.2 MPa is exceeded is the effective cleaning area. Therefore, to obtain satisfactory cleaning results, the laser parameters for removing this level of contamination should be set in the effective cleaning interval. Figs. 18 and 19 illustrate the thermal stress values for cleaning 50 μm and 40 μm contamination, and the effective cleaning parameter interval is derived by comparison with the cleaning threshold. As shown in Fig. 17 to 19, the thermal stress increases linearly with increasing laser power and increases exponentially with decreasing scanning speeds.

In the actual cleaning process, excessive laser power or a slow scanning speed may cause damage to the substrate material, especially in the nonfouling area. Damage caused by direct irradiation of the substrate material is considered during the laser cleaning process. The results of the numerical simulation are shown in Fig. 20. The damage threshold of ceramics obtained from ceramics science is approximately 110 MPa [35], [36]. The damage and safety intervals are obtained by comparing them with the damage threshold values of ceramic materials. Therefore, to avoid damaging the substrate material, the laser parameter range should be set within the safety interval.

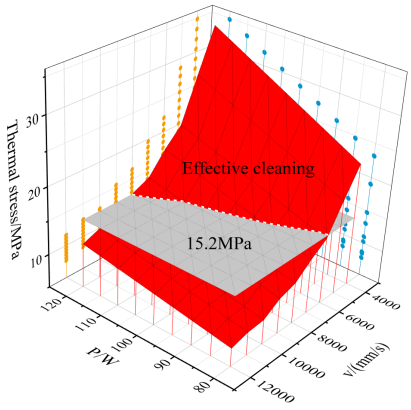

FIGURE 17. Thermal stress with 60 μm contamination.

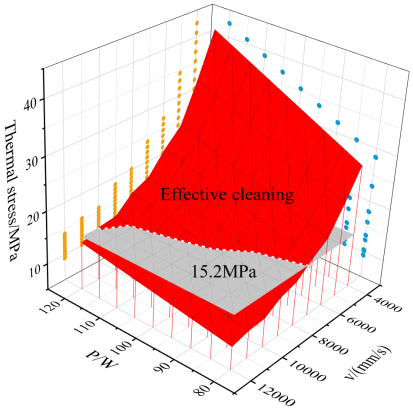

FIGURE 18. Thermal stress with 50 μm contamination.

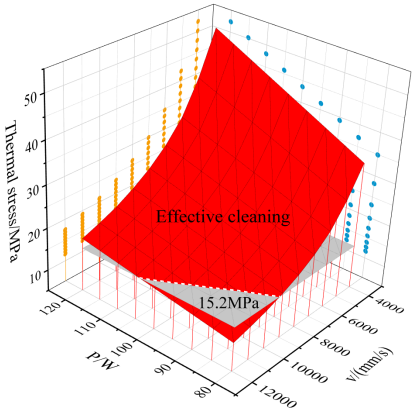

FIGURE 19. Thermal stress with 40 μm contamination.

VII. EXPERIMENTAL RESULTS

To verify the effectiveness of laser cleaning, the laser cleaning of a contamination layer is carried out. An Nd:YAG pulsed laser is used. The laser beam has a wavelength of 1064 nm and a pulse width of 180 ± 20 ns. A schematic diagram of the experimental device is shown in Fig. 21. The experimental device also includes a SCANLABCUBE10 scanning mirror,

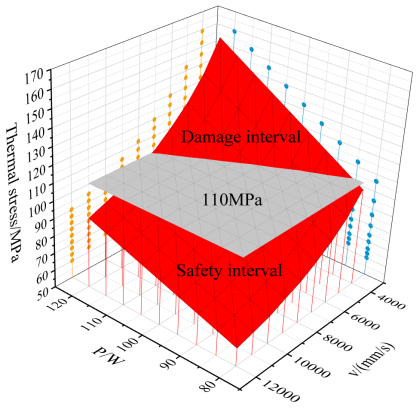

FIGURE 20. Thermal stress without contamination.

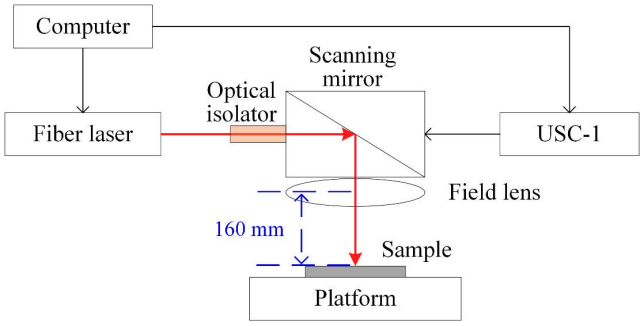

FIGURE 21. Schematic diagram of the experimental device.

a USC-1 scanning mirror controller, a computer and field lens with a focal length of 160 mm. The laser beam is directed by an optical scanning mirror and focused by a quartz field lens perpendicular to the sample surface. Two kinds of samples are tested. One sample is composed of alumina ceramic chips, and its material is the same as that of real insulators. The other sample is composed of ceramic insulators. The flat surface of the substrate material is covered with a contamination layer. The cleaning effect and the influence on the substrate material are investigated.

Fig. 22 shows the samples to be cleaned. The samples were contaminated with artificial pollution according to the instructions in IEC 60507:1991, artificial pollution tests on high-voltage insulators to be used on a.c. systems'. The equivalent salt deposit density (ESDD) is 0.05 mg/cm^2, and the nonsoluble deposit density (NSDD) is taken as 0.25 mg/cm^2.

Fig. 23 illustrates the cleaning effect of samples with different laser power values, and the scanning speed is 8000 mm/s. When the laser output power is 80 W, an outline of the cleaned area can be found. However, only part of the contamination is cleaned off, and a large amount of contamination still remains on the substrate surface. When the laser power increases to 90 W, the outline of the cleaning area can be seen clearly. Most of the contamination layer is cleaned, and only a small amount of contamination particles remains on the substrate surface. The cleaning effect is good.

FIGURE 22. Samples were made by artificial pollution.

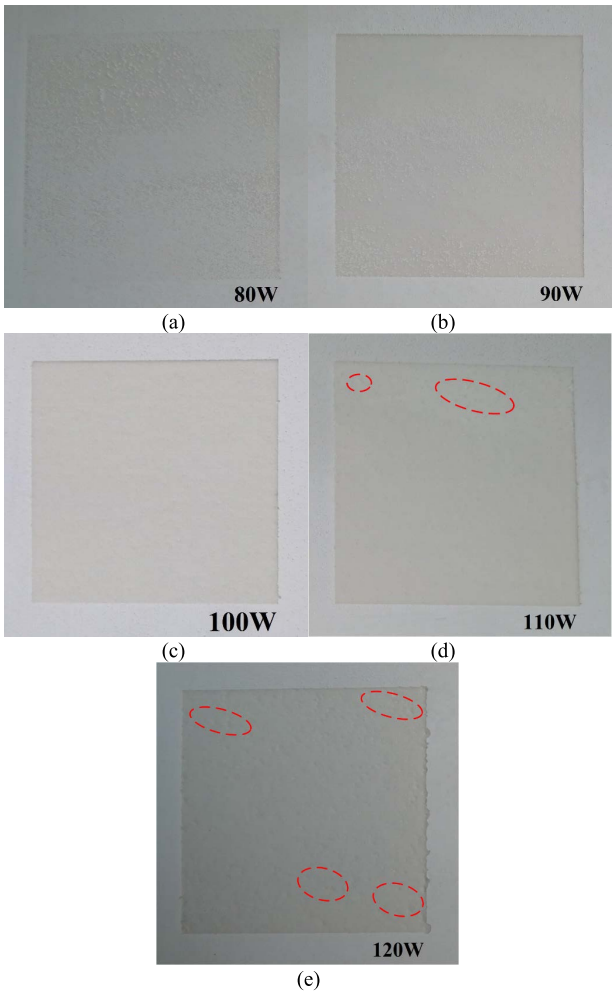

FIGURE 23. Laser cleaning effect with different power values. (a) 80 W, (b) 90 W, (c) 100 W, (d) 110 W, and (e) 120 W.

When cleaning with 100 W power, the contamination was completely cleaned. The cleaning result is satisfactory. The surface of the substrate is completely exposed, and no trace of damage to the substrate surface is found. When the laser

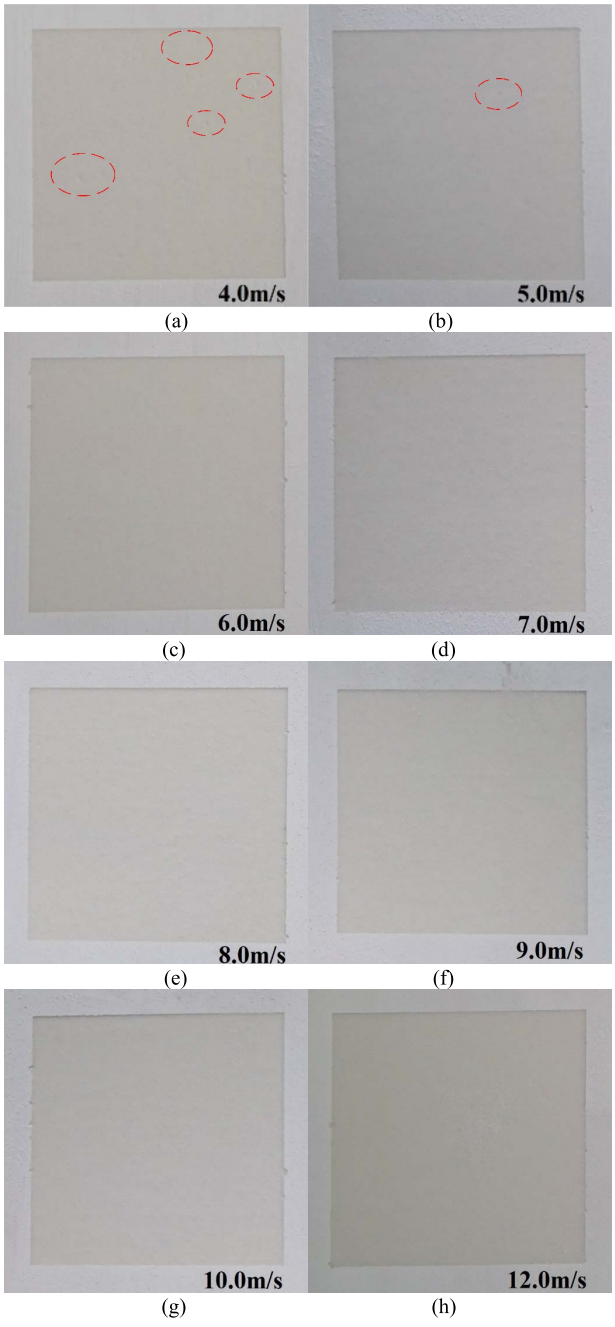

FIGURE 24. Images after laser cleaning at different scanning speeds. (a) 4000 mm/s, (b) 5000 mm/s, (c) 6000 mm/s, (d) 7000 mm/s, (e) 8000 mm/s, (f) 9000 mm/s, (g) 10000 mm/s, and (h) 12000 mm/s.

power is increased to 110 W, the contamination layer is cleaned. However, slight damage was observed on the surface of the substrate material. When the power was increased to 120 W, the contamination layer was cleaned. However, many pits appeared on the surface of the substrate, and the damage was serious. The experimental results show that the laser power has a great influence on the cleaning effect. In the cleaning process, the laser power should be set in the range of 90-100 W to avoid damage to the substrate material.

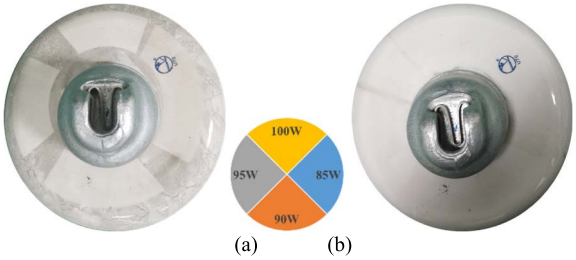

FIGURE 25. Insulator cleaning effect with different laser power values. (a) After cleaning; (b) after wiping.

The samples were cleaned at different scanning speeds, and the results are shown in Fig. 24. A laser beam with a scanning speed within a range of 4000 mm/s to 10000 mm/s can effectively clean off the contamination layer. When the scanning speed increases to 12000 mm/s, most of the contamination is cleaned, but a small number of particles remained. The cleaning effect is acceptable. However, at a scanning speed of 5000 mm/s, partial damage was observed on the surface of the substrate. Laser cleaning can cause damage to the substrate material. To ensure an adequate cleaning effect without damaging the substrate material, the scanning speed should be set in the range of 6000 mm/s to 12000 mm/s with a power of 100 W.

The above simulation and experimental study results show that the contamination layer can be effectively removed by laser cleaning.

To verify the effectiveness of cleaning porcelain insulator surface contamination, laser cleaning tests were carried out on artificially contaminated insulators. The cleaning results are shown in Fig. 25(a) using different power lasers for cleaning. The right area is the area that was cleaned at a power of 85 W. It was found that most of the contamination was removed, but there was still some contamination left on the surface. When the power is increased to 90 W, the contamination layer is almost cleared. When the power is increased to 100 W, the contamination layer is completely removed, and the clean ceramic surface is exposed. After wiping the cleaned insulator, damage to the insulator is observed. The result is shown in Fig. 25(b). It is found that the surface of the insulator is smooth and complete. The results show that the insulator surface is not damaged.

The experimental results show that with a laser power of 90 W $\sim$ 100 W and scanning speed of 8000 mm/s, the insulator surface can be effectively cleaned without causing damage to the porcelain insulator surface.

VIII. CONCLUSION

In this paper, a numerical model for the laser cleaning of contaminated insulators was established. The thermal stress distribution characteristics on the interface, influencing factors and cleaning effect on the ceramic substrate material were investigated. The criteria for the effective removal of the contamination layer were derived.

The numerical simulation results show that the peak value of thermal stress appears at the spot centre and that the

surrounding thermal stress decreases gradually. The thermal stress increases approximately linearly with increasing laser power. In contrast, the thermal stress is approximately inversely proportional to the scanning speed and the thickness of the contamination layer. The theoretical parameter interval for effective cleaning was obtained.

Furthermore, the laser cleaning experimental results show that a laser power of 90-100 W and a scanning speed in the range of 6000-12000 mm/s can effectively remove substrate surface contamination and will not cause damage to the substrate. Through the laser cleaning of artificially coated porcelain insulators, the best cleaning effect was achieved when the laser power was 100 W and the scanning speed reached 6000 mm/s.

REFERENCES

[1] Z. Wang, J. Xu, H. Xiao, W. Zhang, J. Li, and S. Zhan, "Suppression measures of insulator flashover caused by haze flashover," in *Proc. China Int. Conf. Electr. Distrib. (CICED)*, Tianjin, China, Sep. 2018, pp. 566–570.

[2] S. U. Zhiyi and L. I. Qingfeng, "Historical review and summary on measures against pollution flashover occurred in power grids in China," (in Chinese), *Power Syst. Technol.*, vol. 34, no. 12, pp. 124–130, Dec. 2010.

[3] Y. Jiang, "Study on dynamic behavior characteristics of particle on insulator surface under strong electric field," M.S. thesis, Dept. Electron. Eng., Huazhong Univ. Sci. Technol., Wuhan, China, 2019.

[4] Z. Wang, J. Wang, S. Huang, and Y. Fan, "Hot washing of quadruple polluted insulator string on 500 kV transmission line," *High Voltage Eng.*, vol. 40, no. 12, pp. 3688–3694, Dec. 2014, doi: 10.13336/j.1003-6520.hve.2014.12.006.

[5] X. Li, J. Wang, Y. Fan, S. Huang, Y. Liao, and Q. Zhan, "Experimental research on hitting force characteristics of water column in hot washing," *Trans. China Electrotech. Soc.*, vol. 30, no. 9, pp. 124–130, May 2015.

[6] L. Cai, Y. Fan, J. Wang, S. Huang, Y. Liao, and M. Zhou, "Experimental research on hot washing efficiency of 500 kV post insulator," *High Voltage Eng.*, vol. 43, no. 7, pp. 2294–2300, Jul. 2017.

[7] M. M. Daha, M. E. Ibrahim, and M. A. Izzularab, "Effect of washing water flow rate and pollution level on leakage current of a fixed washed high voltage insulator," in *Proc. 18th Int. Middle East Power Syst. Conf. (MEPCON)*, Cairo, Egypt, Dec. 2016, pp. 234–239.

[8] E. Liu and Z. Hua, "Research on optimization method of cleaning parameters of insulator dry ice cleaning robot," in *Proc. IEEE 5th Conf. Energy Internet Energy Syst. Integr. (EI)*, Taiyuan, China, Oct. 2021, pp. 4278–4283, doi: 10.1109/EI252483.2021.9712898.

[9] H. Li, "The development of substation electrical insulators dry ice cleaning robot," M.S. thesis, Dept. Electric. Eng., Inner Mongolia Univ. Technol., Inner Mongolia, China, 2014.

[10] W. Zhou, M. Liu, S. Liu, M. Peng, J. Yu, and C. Zhou, "On the mechanism of insulator cleaning using dry ice," *IEEE Trans. Dielectr. Electr. Insul.*, vol. 19, no. 5, pp. 1715–1722, Oct. 2012, doi: 10.1109/tdei.2012.6311520.

[11] Z. Tang, F. A. N. Yadong, and W. Jianguo, "Influence of live-working washing agents on power frequency flashover voltage of insulator," *High Voltage App.*, vol. 53, no. 8, pp. 181–186, Aug. 2017.

[12] V. A. Parfenov and S. V. Titov, "Technical and technological aspects of laser cleaning for books and documents," in *Proc. IEEE Conf. Russian Young Researchers Electr. Electron. Eng. (EIConRus)*, Saint Petersburg Moscow, Russia, Jan. 2019, pp. 903–906, doi: 10.1109/EIConRus.2019.8657248.

[13] Y. F. Lu, W. D. Song, B. W. Ang, M. H. Hong, D. S. H. Chan, and T. S. Low, "A theoretical model for laser removal of particles from solid surfaces," *Appl. Phys. A, Mater. Sci. Process.*, vol. 65, no. 1, pp. 9–13, Jul. 1997, doi: 10.1007/s003390050533.

[14] N. Arnold, "Theoretical description of dry laser cleaning," *Appl. Surf. Sci.*, vols. 208–209, pp. 15–22, Mar. 2003, doi: 10.1016/s0169-4332(02)01278-3.

[15] C. Liu, G. Feng, G. Deng, C. Wu, K. Chen, and D. Wang, "Temperature field analysis and experiment study about paint irradiated by moving laser based on FEM," *Laser Technol.*, vol. 40, no. 2, pp. 274–279, Mar. 2016.

[16] L. Gao, Z. Jianzhong, S. Qi, L. Huating, Z. Ming, G. Zhaoheng, and Y. Jianian, "Numerical simulation and surface morphology of laser-cleaned aluminum alloy paint layer," *Chin. J. Lasers*, vol. 46, no. 5, pp. 335–343, Mar. 2019, doi: 10.3788/CJL201946.0502002.

[17] G. Zhang, X. Hua, Y. Huang, Y. Zhang, F. Li, C. Shen, and J. Cheng, "Investigation on mechanism of oxide removal and plasma behavior during laser cleaning on aluminum alloy," *Appl. Surf. Sci.*, vol. 506, Mar. 2020, Art. no. 144666, doi: 10.1016/j.apsusc.2019.144666.

[18] J. Yang, J. H. Han, T. Duan, N. C. Sun, C. Guo, G. Y. Feng, and Q. X. Liu, "Mechanical analysis of paint film stripping from aluminum plate surface by means of nanosecond laser," *Laser Technol.*, vol. 37, no. 6, pp. 718–722, Nov. 2013.

[19] Z. Wang, X. Zeng, and W. Huang, "Parameters and surface performance of laser removal of rust layer on A3 steel," *Surf. Coatings Technol.*, vol. 166, no. 1, pp. 10–16, Mar. 2003, doi: 10.1016/s0257-8972(02)00736-3.

[20] G. X. Chen, T. J. Kwee, K. P. Tan, Y. S. Choo, and M. H. Hong, "Laser cleaning of steel for paint removal," *Appl. Phys. A, Solids Surf.*, vol. 101, no. 2, pp. 249–253, Jun. 2010, doi: 10.1007/s00339-010-5811-0.

[21] Y. Xue, W. Wang, X. Wang, J. Wang, G. Li, W. Gao, B. Li, and K. Li, "Laser cleaning technology of 38CrMoAl material surface pollutants," *Infr. Laser Eng.*, vol. 47, no. 7, pp. 73–79, Jul. 2018, doi: 10.3788/irla201847.0706004.

[22] Y. Ye, Y. Qi, L. Qin, Y. Jiang, K. Xiao, H. Wang, X. Luan, X. Cheng, and X. Yuan, "Laser cleaning of contaminations on the surface of stone relics," *Chin. J. Lasers*, vol. 40, no. 9, pp. 90–95, Sep. 2013, doi: 10.3788/CJL201340.0903005.

[23] Y. Qi, Y. Ye, H. Wang, and W. Zhou, "Mechanisms of laser cleaning of contamination on surface of stonework," *Chin. J. Lasers*, vol. 42, no. 6, pp. 99–107, Jun. 2015, doi: 10.3788/cjl201542.0603001.

[24] Y. Ye, B. Jia, J. Chen, Y. Jiang, H. Tang, H. Wang, X. Luan, W. Liao, C. Zhang, and C. Yao, "Laser cleaning of the contaminations on the surface of tire mould," *Int. J. Modern Phys. B*, vol. 31, nos. 16–19, pp. 9–13, Jul. 2017, doi: 10.1142/s0217979217441008.

[25] Y. Qiao, J. Zhao, S. Wang, Z. H. Cai, J. Zhang, and G. X. Zhang, "Laser cleaning and elemental composition analysis of rusty surface," *Laser Infr.*, vol. 48, no. 3, pp. 299–304, Mar. 2018.

[26] W. Xilin, W. Han, X. Xiaoran, J. Zhidong, G. Zhicheng, Z. Lin, and L. Ruihai, "A new method to remove the aging RTV coatings on glass insulators," in *Proc. IEEE Int. Conf. Dielectr. (ICD)*, Montpellier, France, Jul. 2016, pp. 709–711.

[27] Q. Chen, *Laser Material Interaction and Thermal Field Simulation*. Yunnan, China: Yunnan Science and Technology Press, 2001.

[28] D. Savastru, R. Savastru, I. Lancranjan, S. Miclos, and C. Opran, "Numerical analysis of laser paint removal from various substrates," *Proc. SPIE*, vol. 8882, Jun. 2013, Art. no. 88820S.

[29] Y. Tong, "Basic research on mechanism and application of laser removal of metal oxides," Ph.D. dissertation, Dept. Mech. Eng., Jiangsu Univ., Zhenjiang, China, 2014.

[30] H. Peng, "Research on the key factors impacting insulator hot washing cleaning effect," M.S. thesis, Dept. Mech. Eng., Southwest Jiaotong Univ., Chengdu, China, 2014.

[31] H. Li, "Study on the mechanism of dynamic contamination accumulating and its on-line monitoring of external insulation of high voltage transmission line," Ph.D. dissertation, Dept. Elect., South China Univ. Technol., Guangzhou, China, 2012.

[32] Y. F. Lu, W. D. Song, and T. S. Low, "Laser cleaning of micro-particles from a solid surface—Theory and applications," *Mater. Chem. Phys.*, vol. 54, nos. 1–3, pp. 181–185, Jul. 1998, doi: 10.1016/s0254-0584(98)00026-1.

[33] F. Song, W. Zou, and B. Tian, "Model of one-dimensional thermal stress applied in paint removal by Q-switched short pulse laser," *Chin. J. Lasers*, vol. 34, no. 11, pp. 1577–1581, Nov. 2007.

[34] Z. Y. Su and Y. S. Liu, "Comparison of natural contaminants accumulated on surfaces of suspension and post insulators with DC and AC stress in northern China's inland areas," *Power Syst. Technol.*, vol. 28, no. 10, pp. 13–17, May 2004.

[35] Z. Jin, *Engineering Ceramic Materials*. Xian, China: Xi'an Jiaotong Univ. Press, 2000.

[36] *Ceramic and Glass-Insulating Materials—Part 3: Specifications for Individual Materials*, Standard IEC 60672-3, 1997.

XIANQIANG LI (Member, IEEE) was born in Xiangyang, China, in 1973. He received the B.S., M.S., and Ph.D. degrees in high voltage and insulation technology from Wuhan University, Wuhan, China, in 1995, 1998, and 2015, respectively. He is currently a Lecturer at the Department of Electrical Engineering, Wuhan University of Technology, Wuhan. His research interests include lightning protection and grounding technology, external insulation of electrical equipment, transformer modeling, and substation live working.

JI TIAN was born in Enshi, China in 1997. He received the B.S. degree in electrical engineering from China Three Gorges University, Yichang, China, in 2019. He is currently pursuing the M.S. degree with the School of Automation, Wuhan University of Technology. His research interests include high voltage technology, gas discharge, and electrical insulation.

ZHIYUAN MA was born in Suzhou, China, in 1996. He received the B.S. and M.S. degree in electrical engineering from the Wuhan University of Technology, Wuhan, China, in 2018 and 2021, respectively. He is currently working at State Grid Suzhou Power Supply Company. His research interests include high voltage and insulation, and insulator pollution flashover prevention.

WENCHUANG ZHOU was born in Huanggang, China, in 1997. He received the B.S. degree in automation from the Hubei University of Technology, Wuhan, China, in 2018. He is currently pursuing the M.S. degree with the School of Automation, Wuhan University of Technology. His research interests include high voltage, insulation, and laser cleaning insulator contamination.

YUANCHENG QIN was born in Guigang, China, in 1998. He received the B.S. degree in electrical engineering from the Wuhan University of Technology, Wuhan, China, in 2021, where he is currently pursuing the M.S. degree with the School of Automation. His research interests include high voltage technology, gas discharge, and electrical insulation.